Обзор ArXiv/astro-ph, 8-15 сентября 2025

От Сильченко О.К.

ArXiv: 2509.07913

Disclosing Submillimeter Galaxy Formation: Mergers or Secular Evolution?

SIU-WANG CHAN(陳瀟弘) [1,2], YIPING AO [1,2] AND QINGHUA TAN [1,2]

[1] *Purple Mountain Observatory, Chinese Academy of Science, 10 Yuanhua Road, Nanjing 210023, People's Republic of China*
[2] *School of Astronomy and Space Sciences, University of Science and Technology of China, Hefei 230026, People's Republic of China*

ABSTRACT

We analyze the morphology of 125 submillimeter galaxies (SMGs) in the PRIMER-COSMOS field using double Sérsic modeling on JWST NIRCam images across six bands (F150W, F200W, F277W, F356W, F410M and F444W), with SMGs being classified by bulge Sérsic index (*n_bulge*) and bulge-to-total luminosity ratio (B/T). The Kolmogorov–Smirnov test between the bright ($SFR > 175\ M_\odot\ yr^{-1}$) and the faint group ($SFR < 175\ M_\odot\ yr^{-1}$) reveals no significant statistical differences in morphology across bands. However, we notice that SMGs skew towards higher B/T ratios and lower *n_bulge* from shorter to longer wavelengths. In F444W, bright SMGs exhibit higher B/T and lower *n_bulge*, indicating flatter , disturbed bulges, while faint SMGs show lower B/T and higher *n_bulge*. Notably, SMGs with higher B/T tend to have low Sérsic, challenging the local universe dichotomy of classical bulges ($B/T > 0.5$, $n > 4$) versus pseudo-bulges ($B/T < 0.35$, $n < 2$). In the F277W, non-parametric measurements indicate predominantly disk-dominated patterns, with only 24% of SMGs demonstrating merger signatures. After the removal of SMGs with disturbed morphology , the bulge classification scheme in F277W shows pseudo-bulges(21%) and clump migration bulges(16%) from secular evolution , compared to 4% merger-built bulges. Surprisingly , 48% of SMGs defy the classification scheme , showing high $B/T(\sim 0.7)$ but low Sérsic index($n\_bulge \leq 1$). Bars are confirmed in 7% of SMGs. This work suggests that secular evolution takes precedence over major mergers , supporting the idea that isolated evolution fueled by filamentary gas inflow plays a non-negligible role in the SMG bulge formation.

Выборка

covered by HST ACS and WFC3 coverage from CANDELs(N. A. Grogin et al. 2011), providing optical-to-near-infrared data ranging from $0.4\mu m$ to $1.6\mu m$. We excluded filters suffering from the issues of invisibility of the near-infrared counterparts (F090W, F115W) , and those with insufficient resolution for further analysis(F770W, F1800W) , which results in the remaining six bands(F150W, F200W, F277W, F356W, F410M, F444W) with robust detections of the JWST. Since detections in differenct wavelength, we convert the flux detected in different bands to $870\mu m$ via $f_{870\mu m}/f_{obs} = (\nu_{870\mu m}/\nu_{obs})^3$.

In the end , we obtained 125 unique sources detected by ALMA, with the complete catalog 6 in the Appendix. The median of $log_{10}(M_*/M_\odot)$ is $10.98^{+0.53}_{-0.58}$ (16th to 84th percentile) , and the median redshift for our sample is $2.29^{+3.89}_{-1.48}$(16th to 84th percentile) , which is consistent with the typcial redshift range of the SMGs but skews toward higher redshift, dominating fainter end of the SMGs population($S_{870\mu m} = 1.88^{+1.28}_{-0.72}\ mJy$). The physical properties presented in this paper are all retrieved from the $A^3COSMOS$ project (S. Adscheid et al. 2024), in which they performed SED fitting with MAGPHYS, integrating ALMA sub-mm data with extensive ancillary data , including radio (e.g., VLA 1.4 GHz and 3 GHz), far-infrared (e.g., Herschel, Spitzer/MIPS 24 μm), and optical-to-near-infrared photometry. The uncertainties of the photometric redshift conform to $0.06(1 + z)$, which is suitable for statistical measurements but not clusters proximity survey. As for stellar mass , the A3COSMOS paper excludes outliers and unreliable associations , ensuring a robust catalog with a

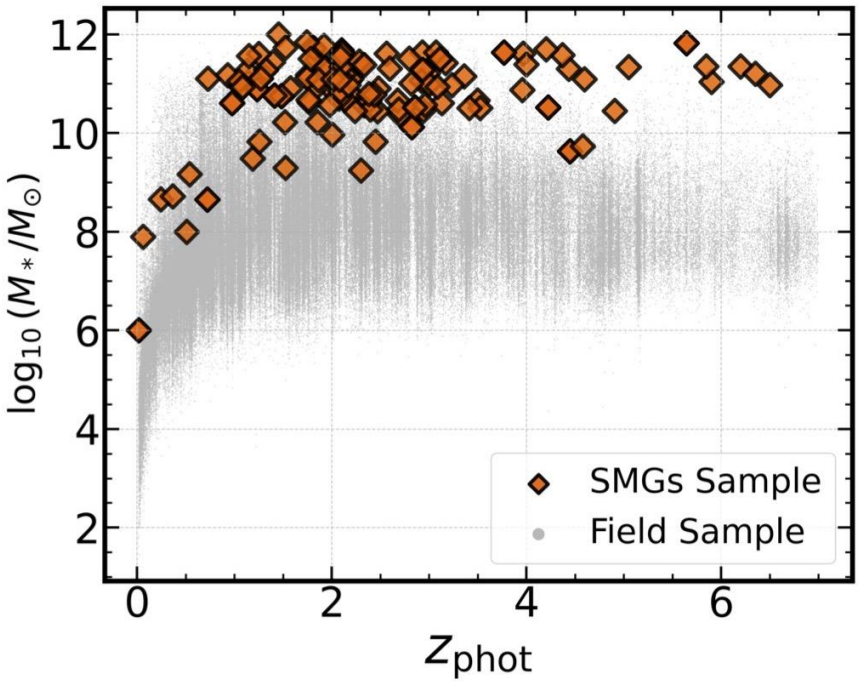

Figure 1. Photometric Redshift vs Stellar Mass for 125 selected SMGs(orange) , and the field sample(gray) in PRIMER-COSMOS field

Не-параметрический анализ морфологии

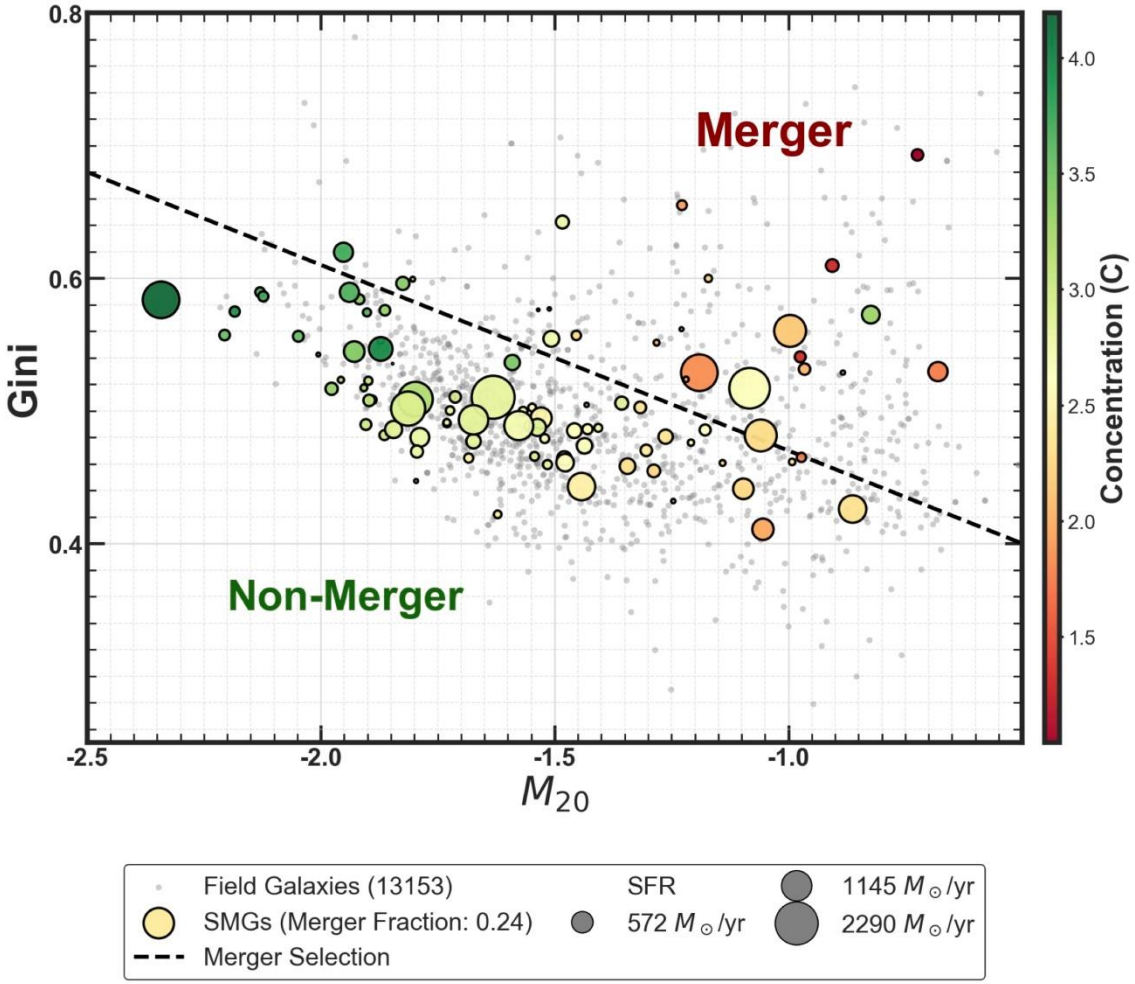

Figure 6. `Gini-M20` relation for both the SMGs and the field galaxies in the PRIMER-COSMOS field , with the dashed line indicating the boundry of the galaxies with merger signatures and those non-mergers , with detailed description in J. M. Lotz et al. (2008).

Изофотный анализ для поиска баров

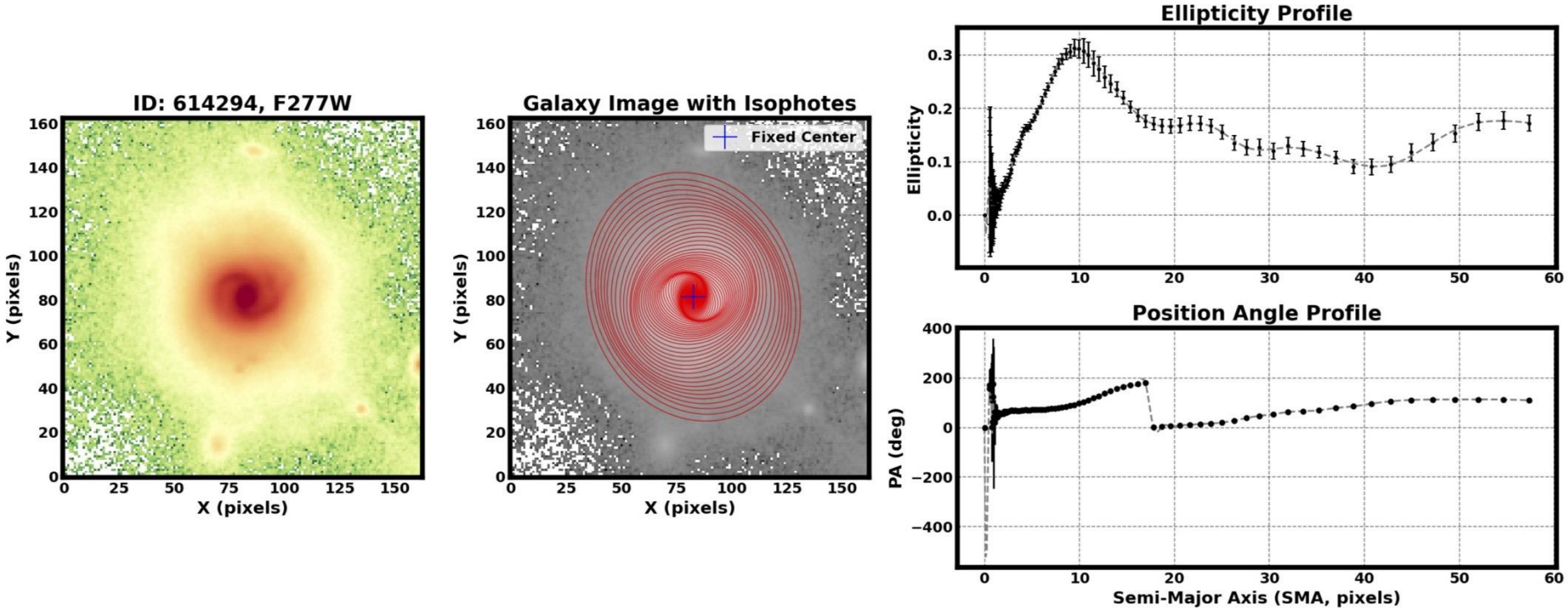

Figure 3. An example of bar identification via ellispe isophotal fitting of source ID: 614294 via ellipse-fitting techniques as an example. The blue cross marks the shared center of isophotes(red).

Эффективные радиусы балджей и дисков при вписывании двойного Сersика

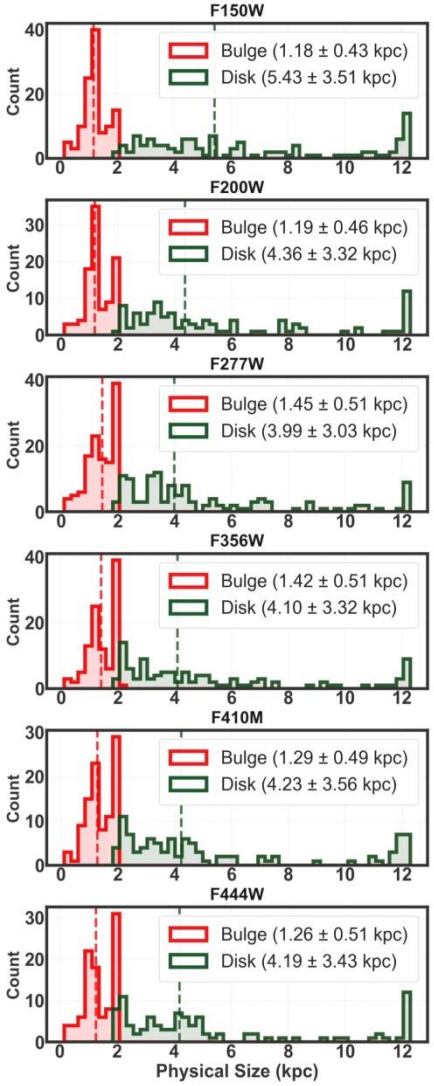

Figure 5. Distribution of the effective radius of bulge(`Re_bulge`) and disk(`Re_disk`) across F150W, F200W, F277W, F356W, F410M, and F444W, with the red and dark blue dotted vertical line indicating the median of the effective radius of the bulge and the disk respectively.

4.1.3. *Properties of the SMGs in different bulge categories*

We highlight the properties of our sample of SMGs categorized by different types of bulges in Table 5. Classical bulges exhibit relatively high stellar mass ($1.6^{+1.1}_{-0.9} \times 10^{11}\ M_\odot$) and elevated star formation rates ($162.2^{+200.9}_{-73.1}\ M_\odot\ \mathrm{yr}^{-1}$). In particular, they show some of the broadest diversity in structural properties , with a bulge-to-total ratio (B/T) of $0.3^{+0.2}_{-0.1}$, a Sérsic index of $n = 4.6^{+1.1}_{-1.9}$, and an effective radius of $R_{\rm eff} = 2.0^{+0.0}_{-0.5}$ kpc.

Within this category, bulges built through major mergers are sites of particularly extreme cases. These systems have high stellar masses ($1.3^{+1.3}_{-0.9}\times10^{11}\ M_\odot$) and SFRs ($152.5^{+273.6}_{-116.6}\ M_\odot\ \mathrm{yr}^{-1}$) , along with the highest median B/T ($0.6^{+0.1}_{-0.0}$) , a high Sérsic index ($n = 4.4^{+1.0}_{-0.2}$) , and compact bulges ($R_{\rm eff} = 1.4^{+0.7}_{-0.7}$ kpc).

Clump-sinking bulges have stellar masses similar to average classical bulges ($1.6^{+0.6}_{-0.4} \times 10^{11}\ M_\odot$) and even higher SFRs ($204.4^{+294.2}_{-95.5}\ M_\odot\ \mathrm{yr}^{-1}$). Structurally , they lie between merger-built bulges and pseudobulges: their B/T is $0.5^{+0.1}_{-0.1}$, Sérsic index is $2.7^{+0.6}_{-0.3}$, and effective radius is $2.0^{+0.1}_{-0.6}$ kpc.

Pseudobulge-hosting SMGs exhibit the lowest median stellar mass among the classified categories ($0.8^{+0.4}_{-0.4} \times 10^{11}\ M_\odot$) and slightly lower SFRs ($151.4^{+137.1}_{-122.5}\ M_o dot\ \mathrm{yr}^{-1}$). Morphologically , they have the lowest B/T ($0.1^{+0.1}_{-0.1}$) , lowest Sérsic indices ($n = 1.4^{+0.8}_{-0.6}$) , and relatively compact bulges ($R_{\rm eff} = 1.1^{+0.6}_{-0.1}$ kpc).

Finally , SMGs with unclassified bulges show moderate stellar masses ($0.9^{+0.9}_{-0.6} \times 10^{11}\ M_\odot$) and the lowest SFRs ($128.8^{+153.3}_{-52.0}\ M_\odot\ \mathrm{yr}^{-1}$). They exhibit the lowest Sérsic indices ($n = 0.7^{+0.2}_{-0.0}$) , intermediate B/T ($0.7^{+0.2}_{-0.2}$) , and modest bulge sizes ($R_{\rm eff} = 1.6^{+0.3}_{-0.3}$ kpc).

(Двойное) Образование балджей

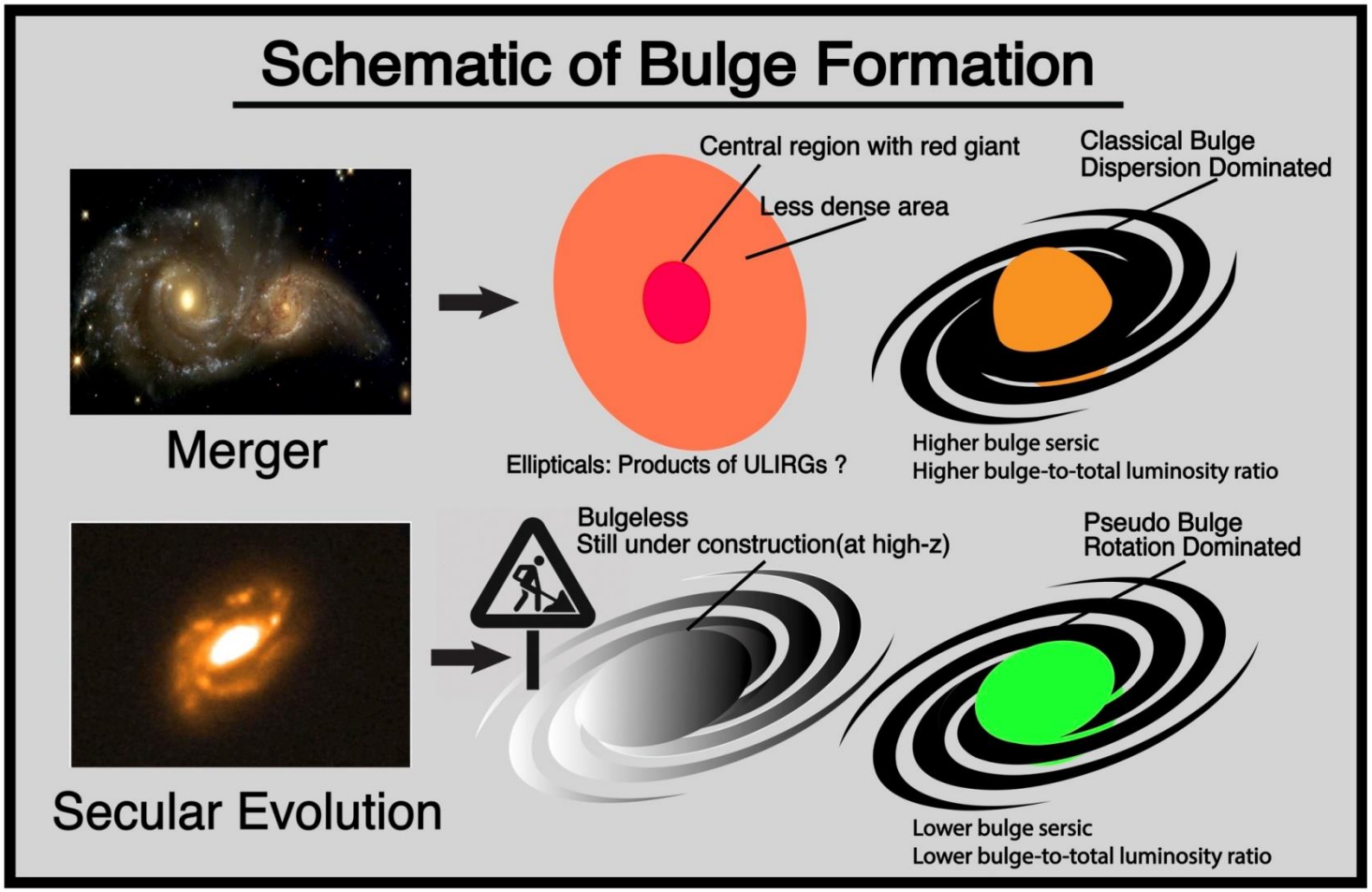

Figure 2. Simple assumptive sketch based on previous studies summarizing the bulge formations in submillimeter galaxies presented in this paper , in which the classical bulge and ellipticals(kinematically hot, high B/T, high Sérsic) are the products of mergers whereas the pseodobulges and the bulgeless galaxies(kinematically cold, low B/T, low Sérsic) are fabricated by degrees in the secular evolution.

Классификация балджей

- Classical Bulge(General Classfication):
  - $n \geq 2$
  - $B/T > 0.2$(Optional, for more restricted purpose)
- Classical Bulge(Merger-built):
  - $n \geq 4$
  - $B/T > 0.5$
- Classical Bulge(Clump sinking):
  - $2 < n < 4$
  - $B/T > 0.2$(Optional, for more restricted purpose)

- Pseudobulge(General Classification):
  - $n < 2$
  - $B/T \leq 0.35$

and please keep in mind that each of these classification criteria has its failure rate ranging from 0% to 20%. To

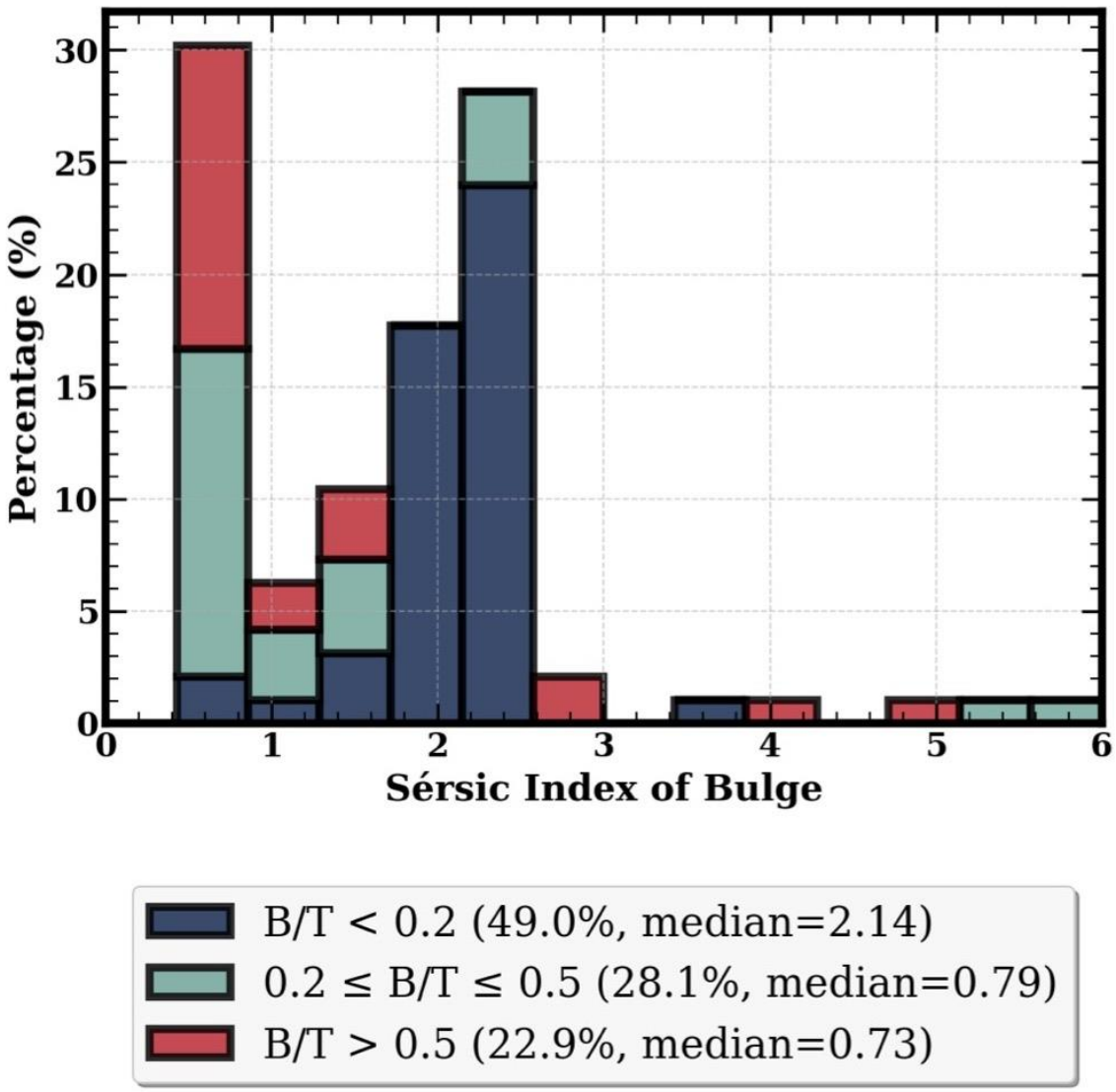

Figure 4. The distribution of bulge Sérsic indices across three B/T bins($B/T < 0.2$, $0.2 \leq B/T \leq 0.5$, $B/T > 0.5$) in band F200W.

Статистика

Band (N)	*Re_bulge* [kpc]	*Re_disk* [kpc]	*n_bulge*	*n_disk*	B/T
F150W (N=116)	$1.18^{+0.26}_{-0.11}$	$5.43^{+4.93}_{-1.85}$	$2.00^{+1.04}_{-1.04}$	$0.69^{+0.44}_{-0.44}$	$0.09^{+0.26}_{-0.26}$
F200W (N=100)	$1.19^{+0.51}_{-0.11}$	$4.36^{+3.35}_{-1.15}$	$1.90^{+1.09}_{-1.09}$	$0.69^{+0.73}_{-0.73}$	$0.22^{+0.31}_{-0.31}$
F277W (N=125)	$1.45^{+0.51}_{-0.38}$	$3.99^{+2.78}_{-0.89}$	$1.47^{+1.85}_{-1.85}$	$0.71^{+1.00}_{-1.00}$	$0.46^{+0.31}_{-0.31}$
F356W (N=106)	$1.42^{+0.60}_{-0.32}$	$4.10^{+2.73}_{-1.30}$	$1.33^{+1.81}_{-1.81}$	$0.71^{+0.97}_{-0.97}$	$0.53^{+0.31}_{-0.31}$
F410M (N=99)	$1.29^{+0.60}_{-0.22}$	$4.23^{+2.88}_{-1.45}$	$1.63^{+1.47}_{-1.47}$	$0.71^{+0.93}_{-0.93}$	$0.47^{+0.34}_{-0.34}$
F444W (N=99)	$1.26^{+0.69}_{-0.20}$	$4.19^{+2.58}_{-1.41}$	$1.48^{+1.51}_{-1.51}$	$0.72^{+0.67}_{-0.67}$	$0.58^{+0.33}_{-0.33}$

Table 1. Summary of physical properties of SMGs across six JWST bands. The columns represent the effective radii of the bulge and disk ($r_{\rm eff,1}$ and $r_{\rm eff,2}$), their Sérsic indices (*n_bulge* and *n_disk*), and the bulge-to-total luminosity ratio (B/T).

Band	B/T Bin	Faint ($SFR < 175\,M_\odot\ \mathrm{yr}^{-1}$)		Bright ($SFR \geq 175\,M_\odot\ \mathrm{yr}^{-1}$)	
		Fraction (%)	***n_bulge* (Median)**	**Fraction (%)**	***n_bulge* (Median)**
F150W	< 0.2	62.3% (43/69)	$2.03^{+0.15}_{-0.54}$	63.8% (30/47)	$2.19^{+0.03}_{-0.13}$
	0.2–0.5	21.7% (15/69)	$1.20^{+0.43}_{-0.46}$	23.4% (11/47)	$1.07^{+0.68}_{-0.40}$
	> 0.5	15.9% (11/69)	$1.25^{+0.45}_{-0.55}$	12.8% (6/47)	$1.06^{+0.12}_{-0.33}$
F200W	< 0.2	44.3% (27/61)	$2.13^{+0.05}_{-0.17}$	53.8% (21/39)	$2.19^{+0.05}_{-0.17}$
	0.2–0.5	29.5% (18/61)	$0.76^{+0.75}_{-0.09}$	28.2% (11/39)	$1.41^{+0.84}_{-0.72}$
	> 0.5	26.2% (16/61)	$0.73^{+0.70}_{-0.06}$	17.9% (7/39)	$0.75^{+0.30}_{-0.08}$
F277W	< 0.2	30.6% (22/72)	$2.15^{+0.13}_{-0.37}$	22.6% (12/53)	$2.22^{+0.05}_{-0.01}$
	0.2–0.5	27.8% (20/72)	$1.28^{+3.00}_{-0.58}$	28.3% (15/53)	$1.47^{+1.47}_{-0.80}$
	> 0.5	41.7% (30/72)	$0.75^{+1.14}_{-0.09}$	49.1% (26/53)	$0.76^{+1.71}_{-0.10}$
F356W	< 0.2	23.8% (15/63)	$2.23^{+1.12}_{-0.06}$	20.9% (9/43)	$2.21^{+1.55}_{-0.02}$
	0.2–0.5	19.0% (12/63)	$3.01^{+1.79}_{-2.02}$	25.6% (11/43)	$1.61^{+4.29}_{-0.94}$
	> 0.5	57.1% (36/63)	$0.72^{+1.20}_{-0.06}$	53.5% (23/43)	$0.69^{+0.33}_{-0.04}$
F410M	< 0.2	28.8% (17/59)	$2.20^{+0.10}_{-0.09}$	25.0% (10/40)	$2.25^{+0.24}_{-0.03}$
	0.2–0.5	20.3% (12/59)	$2.57^{+1.40}_{-1.79}$	30.0% (12/40)	$2.54^{+1.78}_{-1.84}$
	> 0.5	50.8% (30/59)	$0.68^{+0.61}_{-0.02}$	45.0% (18/40)	$0.70^{+0.35}_{-0.04}$
F444W	< 0.2	28.8% (17/59)	$2.21^{+1.00}_{-0.10}$	20.0% (8/40)	$2.24^{+1.14}_{-0.02}$
	0.2–0.5	18.6% (11/59)	$3.22^{+1.54}_{-0.84}$	15.0% (6/40)	$4.35^{+0.48}_{-1.22}$
	> 0.5	52.5% (31/59)	$0.67^{+0.85}_{-0.01}$	65.0% (26/40)	$0.68^{+0.24}_{-0.03}$

Table 4. Distribution of bulge Sérsic index *n_bulge* in B/T bins for faint ($SFR < 175\,M_\odot\ \mathrm{yr}^{-1}$) and b ($SFR \geq 175\,M_\odot\ \mathrm{yr}^{-1}$) SMGs in different JWST bands. Fractions in each bin are shown along with the median *n_b* and asymmetric errors.

Band	**Bulge (*Re_bulge*/ kpc)**			**Disk (*Re_disk*/ kpc)**		
	SFR $< 175\ M_\odot\ \mathrm{yr}^{-1}$	SFR $\geq 175\ M_\odot\ \mathrm{yr}^{-1}$	P-value	SFR $< 175\ M_\odot\ \mathrm{yr}^{-1}$	SFR $\geq 175\ M_\odot\ \mathrm{yr}^{-1}$	P-value
F150W	1.17 ± 0.05	1.11 ± 0.06	0.354	4.81 ± 0.40	6.28 ± 0.53	0.065
F200W	1.19 ± 0.06	1.14 ± 0.06	0.141	4.23 ± 0.38	5.05 ± 0.59	0.268
F277W	1.30 ± 0.06	1.50 ± 0.06	0.335	3.75 ± 0.29	4.43 ± 0.47	0.072
F356W	1.28 ± 0.07	1.47 ± 0.07	0.598	3.74 ± 0.35	4.96 ± 0.57	**0.020**
F410M	1.16 ± 0.06	1.34 ± 0.07	0.396	3.81 ± 0.37	4.61 ± 0.65	**0.043**
F444W	1.20 ± 0.07	1.35 ± 0.08	0.725	3.97 ± 0.36	4.62 ± 0.62	**0.017**

Table 3. Effective radii for bulges (*Re_bulge*) and disks (*Re_disk*) across six bands, split by SFR (in $M_\odot\ \mathrm{yr}^{-1}$). Bold p-values ($< 0.05$) show disks expand as the star formation rate rises.

Bulge Type (N)	**Stellar Mass** ($10^{11} M_\odot$)	**SFR** ($M_\odot\ \mathrm{yr}^{-1}$)	**B/T**	**Sérsic n**	$R_{\rm eff}$ (kpc)
Classical Bulge (N=27)	$1.6^{+1.1}_{-0.9}$	$162.2^{+200.9}_{-73.1}$	$0.3^{+0.2}_{-0.1}$	$4.6^{+1.1}_{-1.9}$	$2.0^{+0.0}_{-0.5}$
Major Merger Bulge (N=4)	$1.3^{+1.3}_{-0.9}$	$152.5^{+273.6}_{-116.6}$	$0.6^{+0.1}_{-0.0}$	$4.4^{+1.0}_{-0.2}$	$1.4^{+0.7}_{-0.7}$
Clump Sinking Bulge (N=16)	$1.6^{+0.6}_{-0.4}$	$204.4^{+294.2}_{-95.5}$	$0.5^{+0.1}_{-0.1}$	$2.7^{+0.6}_{-0.3}$	$2.0^{+0.1}_{-0.6}$
Pseudo Bulge (N=21)	$0.8^{+0.4}_{-0.4}$	$151.4^{+137.1}_{-122.5}$	$0.1^{+0.1}_{-0.1}$	$1.4^{+0.8}_{-0.6}$	$1.1^{+0.6}_{-0.1}$
Unclassified Bulge (N=47)	$0.9^{+0.9}_{-0.6}$	$128.8^{+153.3}_{-52.0}$	$0.7^{+0.2}_{-0.2}$	$0.7^{+0.2}_{-0.0}$	$1.6^{+0.3}_{-0.3}$

Table 5. Median of the physical properties by bulge type, with the lower and upper bounds corresponding to the 25th and 75th percentiles. All values are rounded to one decimal place.

Происхождение балджей

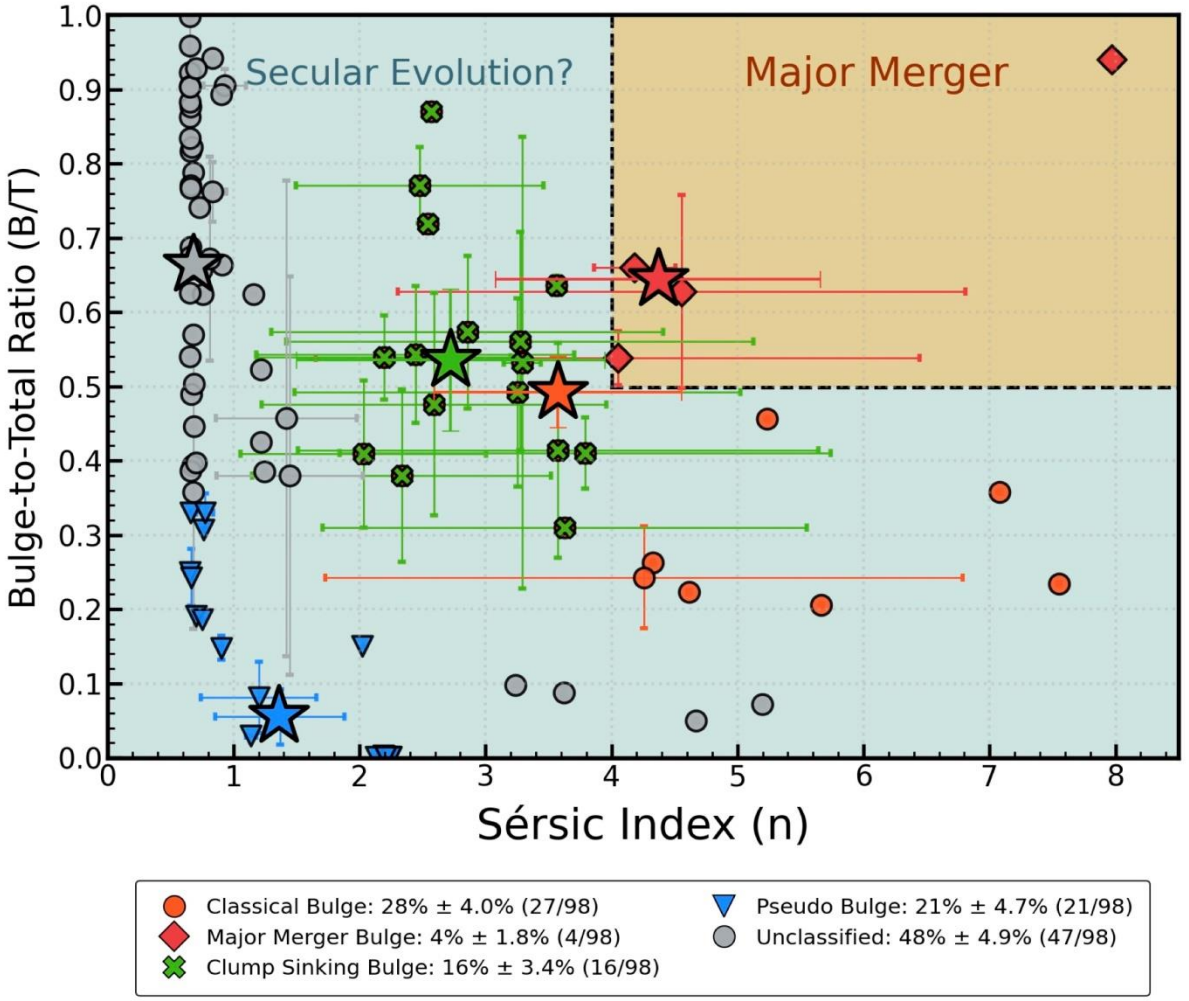

Figure 7. The distribution of different types of bulges based on the classification scheme using sérsic index and bulge-to-total luminosity ratio on band F277W after the removal of the strongly disturbed SMGs , with the big star symbols showing the median of each group.

Заключение:

- Только ~20% (24%) возможных мержеров (и скорее малых).
- Больше половины балджей (76%?)– продукт секулярной эволюции
- Секулярная эволюция= clump sinking (n~2) либо радиальное стекание газа из диска (n=1).
- В половине регулярных дисков (43%) подозревается присутствие бара.
- Чем массивнее галактика, тем менее классический у нее балдж.

Kinematics of the lens host S0 galaxy NGC 1553: role of secular processes

Saili Keshri[1,2], Sudhanshu Barway[1], and Francoise Combes[3]

[1] Indian Institute of Astrophysics, Kormangala II Block, Bengaluru, India, 560034
e-mail: saili.keshri@iiap.res.in
[2] Department of Physics, Pondicherry University, R.V.Nagar, Kalapet, Puducherry, India, 605014
[3] Observatoire de Paris, LUX, College de France, CNRS, PSL University, Sorbonne University, F-75014 Paris, France

September 15, 2025

ABSTRACT

We present an investigation of the central structure of the S0 galaxy NGC1 553, to understand its origin and the underlying dynamical processes that shape it. The high-resolution integral field spectroscopic data from the Multi-Unit Spectroscopic Explorer (MUSE) reveal a well-ordered rotation pattern, consisting of a rapidly rotating nuclear disc that is somewhat decoupled from the main disc, together with an inner lens; we collectively refer to these structures as the "disc-lens". The central peak in the velocity dispersion indicates the presence of a classical bulge. The nuclear disc is dynamically colder than the surrounding disc, while the lens is dynamically hotter. The higher-order Gauss–Hermite moments, h_3 and h_4, further characterise the stellar kinematics. An anti-correlation between the line-of-sight velocity and skewness (h_3) is consistent with regular rotation. In contrast, the ring-like enhancement in kurtosis (h_4) confirms the presence of the nuclear disc component. Unsharp masking of *HST* images (Erwin et al. 2015) reveals a nuclear bar and faint spiral structures within the central ∼10 arcsec, supporting the role of secular evolution. The mass-weighted stellar age map shows an old stellar population in the central regions, with high metallicity that suggests the in-situ formation of the disc–lens from disc material. We discuss possible formation scenarios for the disc–lens, including both minor mergers and secular processes, and examine the influence of the Dorado group environment on NGC 1553. Our findings suggest that the disc–lens in NGC 1553 formed during the early stages of the galaxy's evolution. However, its subsequent development has been shaped by internal and external processes. These results provide new insights into the origin and evolution of kinematically distinct substructures in S0 galaxies.

Центральная галактика группы Dorado

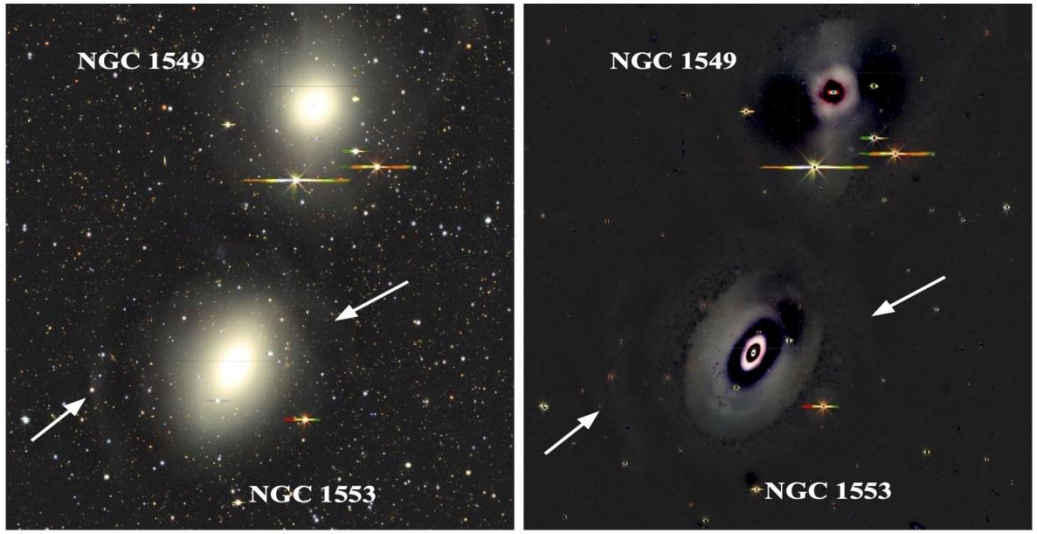

Fig. 1. DECaLS color composite image (left) and residual image (right) of NGC 1553 and nearby galaxy NGC 1549. The white arrow in both images represents the faint shell feature in NGC 1553. North is oriented upward, and east is to the left. The size of the bow is 22 arcmin in each panel.

Table 1. Properties of NGC 1553. The morphology is taken from Buta et al. (2015) and the distance is adopted from Blakeslee et al. (2001). Right Ascension and Declination of the galaxy are taken from NASA/IPAC Extragalactic Database2. Galaxy inclination and disc position angle are adopted from Erwin et al. (2015).

Parameter	Value
Morphology	SA(rl,nrl,nb)0+
Distance (D) [Mpc]	18.5
Right Ascension (J2000) [Deg]	64.043484
Declination (J2000) [Deg]	-55.780005
Inclination angle [Deg]	48
Position angle of disc photometric axis [Deg]	152

S4G: NGC 1553

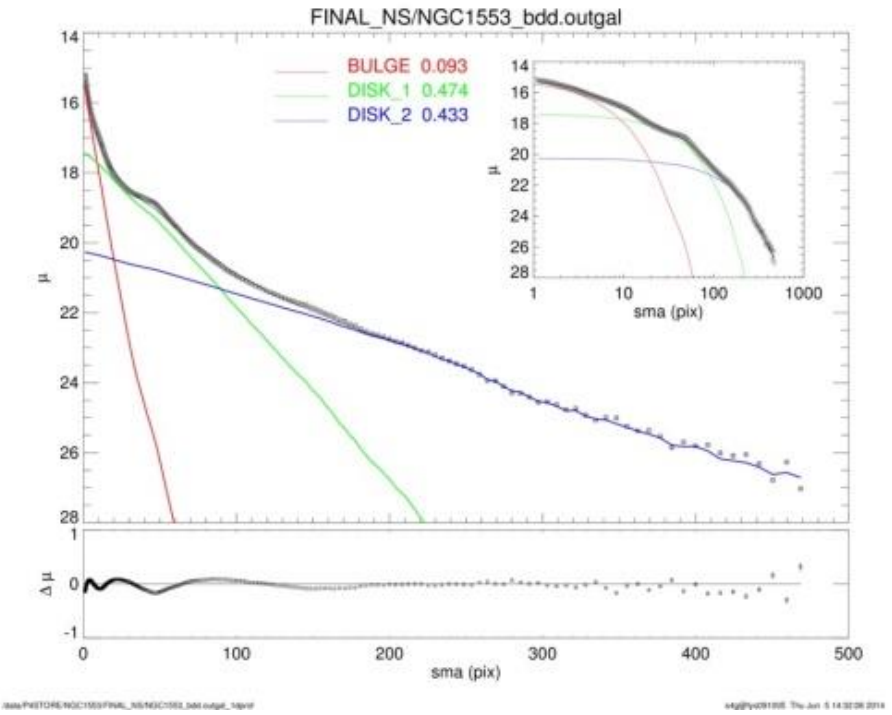

- В данном случае, модель с двухярусным диском; но линза в остатках видна

MUSE: кинематика

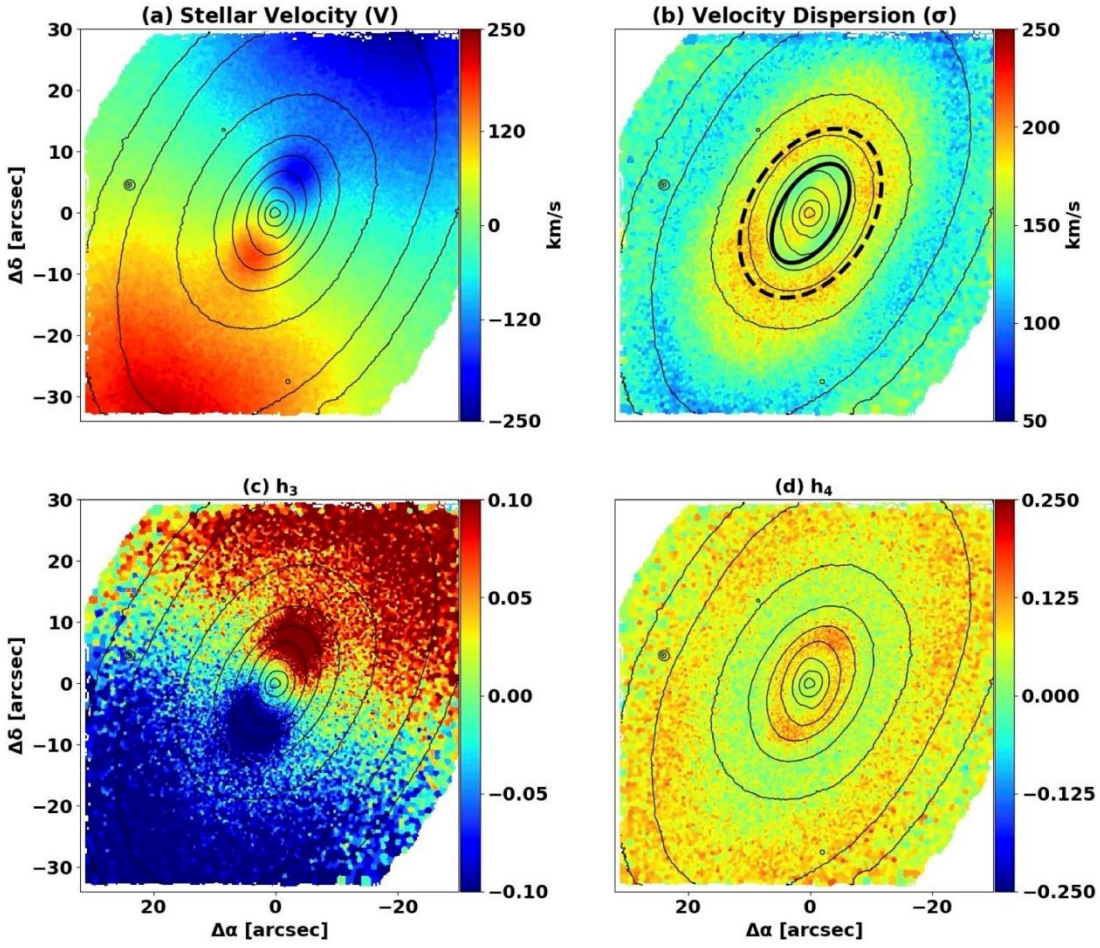

Fig. 2. Stellar kinematic maps of NGC 1553 derived from the MUSE data cube using the GIST pipeline. The line-of-sight (LOS) stellar velocity (V) distribution is presented in the top-left panel, while the corresponding stellar velocity dispersion (σ) map is shown in the top-right panel. The nuclear disc is outlined by the solid black ellipse, while the dashed ellipse indicates the hot inner lens. The third (h_3) and fourth (h_4) Gauss-Hermite velocity moments are displayed in the bottom-left and bottom-right panels, respectively. The overlaid contours, extracted from the MUSE intensity maps, are spaced at uniform intervals of 0.2 mag. The orientation is such that the North is up, and the East is to the left.

Холодные-горячие спаксели

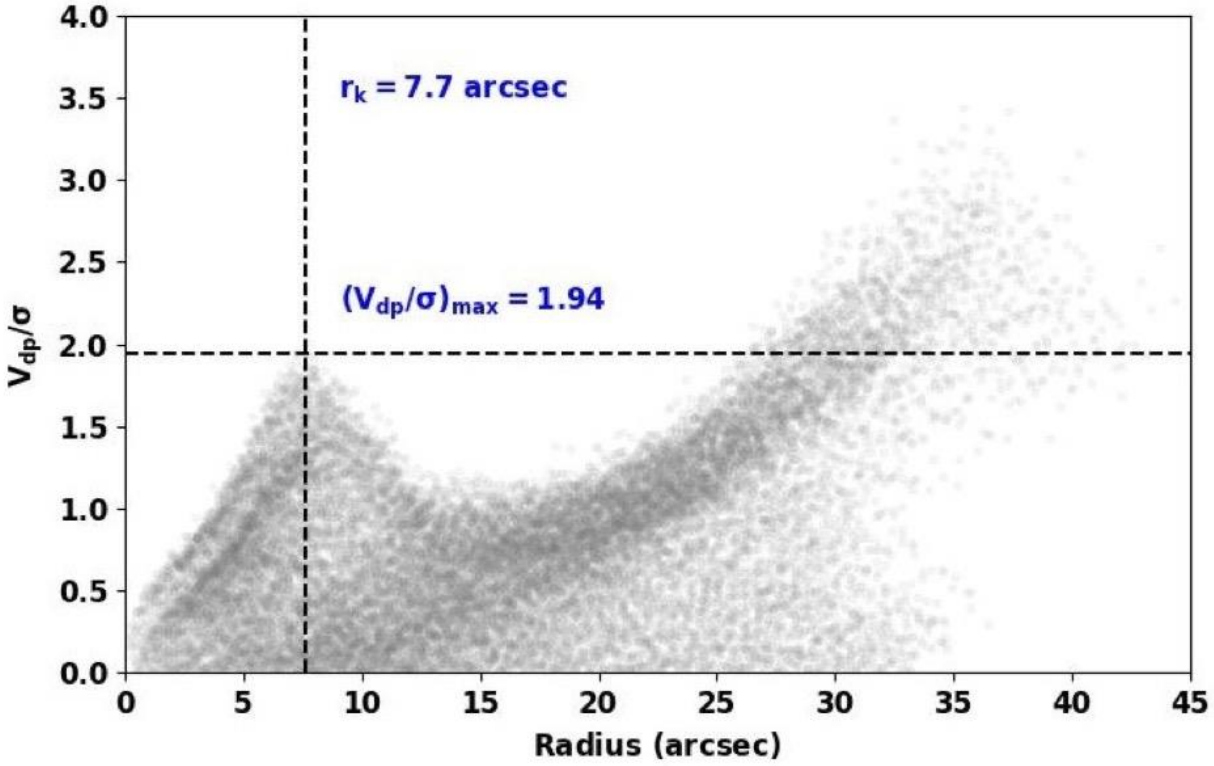

Fig. 4. Deprojected radial profiles of V/σ at each Voronoi bin, with velocity (V) corrected for inclination. The peak value V_{dp}/σ and the radius at which this peak is located (r_k) are shown with the horizontal and vertical dashed lines, respectively, and the corresponding values are also given.

MUSE: свойства звездного населения

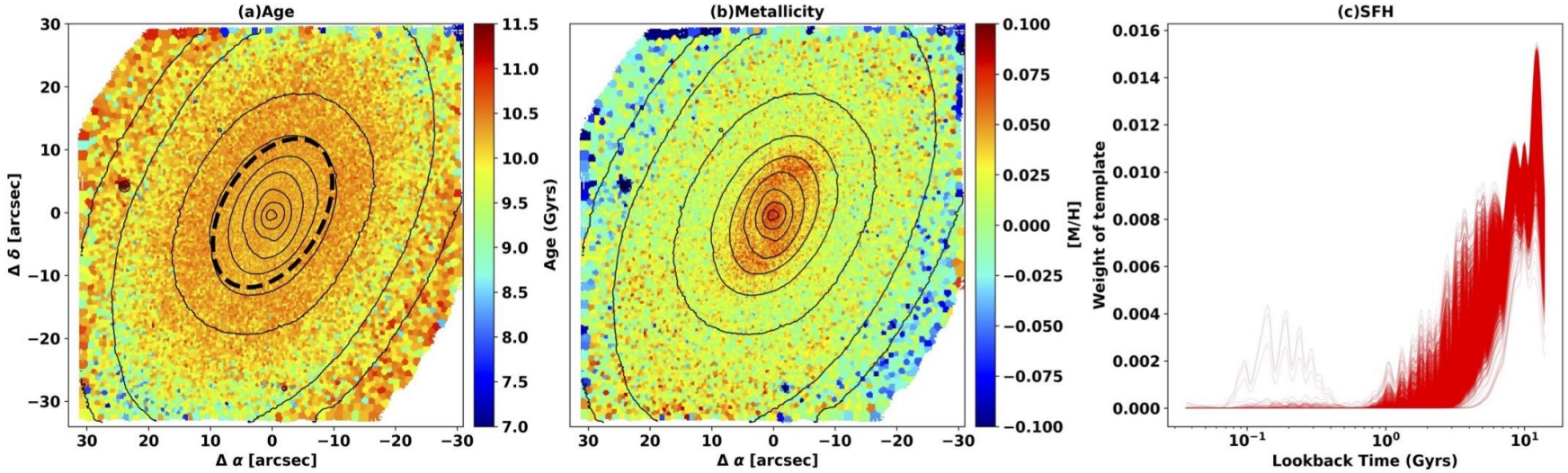

Fig. 5. Mass-weighted stellar age map (left) and stellar metallicty map (middle) of NGC 1553 derived from the Voronoi-binned MUSE data cube. Overlaid black contours represent isophotes from the MUSE white-light image, spaced at intervals of 0.2 mag. The dashed black ellipse marks the central 13 arcsec region corresponding to the nuclear disc-lens. North is up and east is to the left. The star formation history (SFH) is shown on the right, where each profile represents the SFH of an individual bin.